2015

Sample-dependent first-passage-time distribution in a disordered medium

Liang Luo
Beijing Computational Science Research Center, lvquanxia@163.com

Lei-Han Tang
Department of Physics, Hong Kong Baptist University, lhtang@hkbu.edu.hk

Sample-dependent first-passage-time distribution in a disordered medium

Liang Luo[1] and Lei-Han Tang[1,2]
[1]*Beijing Computational Science Research Center, Beijing 100094, China*
[2]*Department of Physics and Institute of Computational and Theoretical Studies, Hong Kong Baptist University, Hong Kong*
(Received 7 April 2015; revised manuscript received 26 July 2015; published 16 October 2015)

Above two dimensions, diffusion of a particle in a medium with quenched random traps is believed to be well described by the annealed continuous-time random walk. We propose an approximate expression for the first-passage-time (FPT) distribution in a given sample that enables detailed comparison of the two problems. For a system of finite size, the number and spatial arrangement of deep traps yield significant sample-to-sample variations in the FPT statistics. Numerical simulations of a quenched trap model with power-law sojourn times confirm the existence of two characteristic time scales and a non-self-averaging FPT distribution, as predicted by our theory.

DOI: 10.1103/PhysRevE.92.042137 PACS number(s): 05.40.−a, 02.50.−r, 87.16.dj, 87.10.Mn

I. INTRODUCTION

The diffusive motion of macromolecules is an essential part of cellular life. It controls the speed of a large number of cellular processes such as signaling, assembly of protein complexes and molecular machines, and exit of mRNAs from the cell nucleus [1–3]. Recent advances in *in vivo* single-molecule imaging have greatly enriched our knowledge of thermally driven transport in the heterogeneous intracellular medium. Experimental measurements have generally indicated a subdiffusive behavior of fluorescently tagged particles in the cytoplasm and the nucleoplasm, as well as on the plasma membrane [4–6]. The origin of the observed anomalous phenomenon is still much debated.

Hitherto, the statistical characteristics of measured particle trajectories have mostly been interpreted using one of the three theoretical models: the fractal Brownian motion with temporal correlation of particle displacements [7–11], the continuous-time random walk (CTRW) with power-law sojourn times [12,13], or the obstructed diffusion caused by organelles in the diffusion path [14,15]. While these models present different scenarios for the cause of subdiffusive scaling of particle displacement with time, they do not take into account the quenched nature of the intracellular medium. For diffusive transport across length scales larger than or comparable to the size of chromosomes, endoplasmic reticula [16], and other organelles, the environment is usually static during the passage of a tracked particle. In such a situation, one expects significant sample-to-sample variations whose statistical mechanical characterization is challenging [17].

One of the well-known models in this context is the quenched trap model (QTM) defined by a set of hopping rates τ_i^{-1} out of sites i on a d-dimensional lattice [18–23], as illustrated in Fig. 1. The time constants τ_i are quenched random variables drawn from a distribution $P_s(\tau)$. Above the critical dimension $d_c = 2$ for returning walks, it is generally expected that the QTM has the same scaling properties as the CTRW where τ_i is reassigned according to the distribution $P_s(\tau)$ upon each visit to site i. The argument was formalized in a renormalization group analysis by Machta [19].

Indications that the scaling properties of the QTM and that of the CTRW may not be identical in high dimensions can be found from previous studies of the first-passage time (FPT) between start and target sites in a confined geometry. The FPT has been suggested to be an important characteristic for understanding reaction kinetics inside a cell [24,25]. Consider a simple example illustrated in Fig. 1 where the start site is at the center of a sphere of radius R and the target is any site on the surface of the sphere. For this geometry and a power-law distribution $P_s(\tau) \sim \tau^{-\mu-1}$ of trapping times τ_i, the mean FPT was shown to scale with R as $\tau_Q \sim R^{d/\mu}$ [18,26]. In comparison, for $\mu < 1$, the typical FPT of the corresponding CTRW is given by $\tau_{\rm typ} \sim R^{2/\mu}$, while the mean FPT diverges. Since the mean FPT tends to be dominated by rare events when the distribution has a fat tail, the above results suggest a qualitatively different tail of the FPT distribution in the two models.

In this paper we develop an analytic scheme to characterize the full FPT statistics in the QTM and to investigate its sample-to-sample fluctuations. Simple physical arguments are presented to reveal the subtle differences in the rare-event statistics between the quenched and annealed systems. The two time scales, $\tau_{\rm typ} \sim R^{2/\mu}$ for the longest trapping time on a typical FPT trajectory and $\tau_Q \sim R^{d/\mu}$ for the longest trapping time in the entire system, arise naturally from the discussion. Based on these understandings, we propose a decomposition scheme that expresses the FPT distribution as an ordered sum of exponentials associated with deepest traps in a given sample. Variations in the strength and location of these traps give rise to sample-to-sample fluctuations in the tail of the FPT distribution, which we characterize analytically. The analytic results are shown to be in excellent agreement with numerical simulations of the two models.

The paper is organized as follows. In Sec. II we define the quenched trap model and mention a few of its basic properties. Section III presents our analytic calculations of the FPT distribution from the point of view of rare-event statistics. Section IV contains results from numerical simulations of the two models, highlighting sample-to-sample variations in the QTM. A brief summary is given in Sec. V.

II. QUENCHED TRAP MODEL

The quenched trap model can be formulated as a Markov process for a diffusing particle whose states are sites on

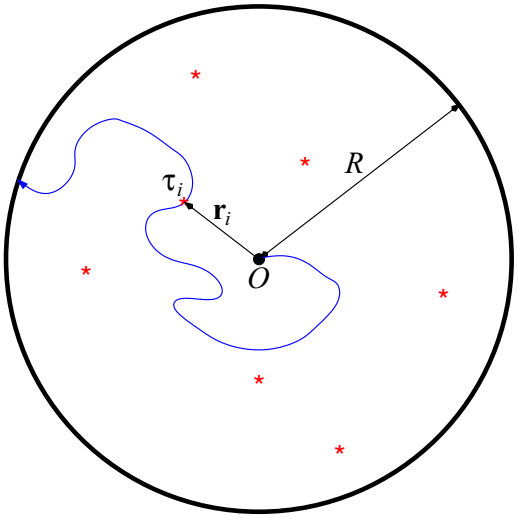

FIG. 1. (Color online) First-passage trajectory (blue line) of a diffusing particle in a quenched environment with deep traps (red dots).

a d-dimensional hypercubic lattice with a lattice constant a. The transition rate from site i to a neighboring site j is given by $W_{i\to j} = (2d)^{-1}\tau_i^{-1}$. The hopping rate $k_i = \tau_i^{-1}$ out of site i can be associated with a site energy V_i (<0) through the Arrhenius law $k_i = \omega_0 \exp(V_i/T)$, where ω_0 is the attempt rate and T the ambient temperature. Of special interest is when the site energies V_i are exponentially distributed

$$P(V) = T_g^{-1} e^{V/T_g} \quad (V < 0). \tag{1}$$

Consequently, the distribution of τ_i follows a power law

$$P_s(\tau) = \mu\omega_0^{-\mu}\tau^{-\mu-1} \quad \left(\tau > \omega_0^{-1}\right). \tag{2}$$

Here the exponent $\mu = T/T_g$. Below we will choose $\tau_0 \equiv \omega_0^{-1}$ as the unit of time unless otherwise specified.

The QTM with a power-law distribution of sojourn time constants (2) offers a plausible description of the diffusion of a macromolecule in the aqueous cellular environment. On short time scales, the molecule is trapped in a certain volume of its size due to either nonspecific binding or the cage effect as in colloidal glass. It has been argued that the Gumbel distribution approximated by (1) is often encountered when multiple factors of comparable strength contribute to the trapping energy V_i [27]. On longer time scales, after breaking off from the trap, the particle diffuses normally until it falls into another trap. In this scenario, the path taken by the molecule is simply a normal random walk, although the journey time may have a very broad distribution. The lattice constant a can be taken to be the linear size of a correlated volume in the medium, beyond which the local potential V_i on the diffusing particle changes to a substantially different value. The time constant τ_0 should be chosen accordingly so that (2) provides an adequate description for hopping between neighboring sites.

According to Eq. (1), the site energies are not bounded from below. However, in a given realization of the disorder, there will be a deepest trap at energy $V_Q = \min_i\{V_i\}$. Let $\mathcal{V} \simeq R^d$ be the volume of the system and $\mathcal{N} = \mathcal{V}/a^d$ be the number of independent sites. The cumulative distribution of V_Q is given by

$$C_V(V_Q,\mathcal{N}) = 1 - (1 - e^{V_Q/T_g})^{\mathcal{N}} \simeq 1 - \exp(-\mathcal{N}e^{V_Q/T_g}) = \hat{C}_V\left(\frac{V_Q}{T_g} + \ln\mathcal{N}\right), \tag{3}$$

where the scaling function $\hat{C}(u) = 1 - \exp(-e^u)$. Therefore, the mean of V_Q decreases logarithmically with $\mathcal{N}$ but its variance remains constant. Consequently, the energy difference between the deepest and the second deepest trap, which can be approximated by the difference in V_Q in two independent realizations of the disorder, is finite and independent of $\mathcal{N}$. The corresponding trapping time constant

$$\tau_Q(R) = \tau_0 \exp(-V_Q/T) \simeq \tau_0(R/a)^{d/\mu} \tag{4}$$

is greater than the second longest time by a factor.

III. ANALYTIC CALCULATION OF THE FIRST-PASSAGE-TIME DISTRIBUTION

For diffusion-limited biochemical reactions inside a cell, one is interested in the FPT of a molecule from its birth place to the reaction site. In this work we focus on the statistics of the FPT for individual cells. To simplify the discussion, we adopt the simplest geometry as illustrated by Fig. 1, where the molecule is launched from the origin at $t = 0$, and examine the distribution $F(t,R)$ of the FPT t to an enclosing spherical surface of radius R. Nevertheless, our approach can be adapted to more general geometries as considered by Bénichou *et al.* [24] using results from the lattice random walk theory [28,29].

A. Continuous-time random walk

If the sojourn times of the diffusing particle at a given site are not distributed in a site-dependent manner but instead follow a common distribution such as Eq. (2), the corresponding stochastic process is known as the continuous-time random walk [12,18]. The CTRW can be considered as an annealed version of the QTM, with the important difference that the statistics of the journey time is independent of the path taken. This subordination property allows one to write

$$F_{\mathrm{CTRW}}(t,R) = \sum_N A_N(R) f_N(t), \tag{5}$$

where $A_N(R)$ is the probability for a lattice random walker to reach the boundary for the first time in N steps and $f_N(t)$ is the probability distribution function of the journey time $t_N = \sum_{i=1}^N t_i$. Under the continuum approximation at large N (which plays the role of time) and R, the lattice random walk is described by the diffusion equation, which, under the substitutions $x \to Rx$ and $N \to R^2N$, yields the scaling solution

$$A_N(R) = R^{-2}\hat{A}_d(NR^{-2}), \tag{6}$$

where the FPT probability density function $\hat{A}_d(u)$ is peaked around $u_{\max} \simeq 1$ and decays exponentially at large u. On the other hand, $f_N(t)$ exhibits a fat tail when the sojourn times t_i are distributed according to (2).

A particularly interesting case is $\mu < 1$, where the mean sojourn time $t_s = \int_0^\infty t P_s(t)dt$ diverges [18,23]. In such a situation, the sum t_N is dominated by the largest term $t_{\max}$

whose typical value grows faster than linear in N. The latter can be seen from the cumulative distribution of $t_{\max}$,

$$\text{Prob}(t_{\max} > t) = 1 - \prod_{i=1}^{N} \text{Prob}(t_i < t) = 1 - (1 - t^{-\mu})^N \simeq 1 - \exp(-Nt^{-\mu}). \quad (7)$$

In Appendix A we show that, in this case, the tail of the distribution of t_N becomes identical to that of $t_{\max}$,

$$f_N(t) \approx P_N(t_{\max} = t) = N\mu(1 - t^{-\mu})^{N-1} t^{-\mu-1}. \quad (8)$$

Equations (7) and (8) show that the distributions of $t_{\max}$ and of t_N are both peaked around $\tau_{\text{typ}} \simeq N^{1/\mu}$ and have the expected power-law tail beyond τ_{typ}. Combining Eqs. (5)–(8), we obtain the subdiffusive scaling [18,30]

$$F_{\text{CTRW}}(t,R) \simeq \int \frac{dN}{R^2} \hat{A}_d\left(\frac{N}{R^2}\right) N\mu \exp\left(-\frac{N}{t^\mu}\right) t^{-\mu-1} = \mu R^2 t^{-\mu-1} \Phi(tR^{-2/\mu}) \quad (\mu < 1). \quad (9)$$

Here $\Phi(z) = \int_0^\infty du\, u \hat{A}_d(u) \exp(-u/z^\mu)$ increases monotonically with z and saturates to $\Phi_\infty \equiv \Phi(\infty)$ at large z. Hence $F_{\text{CTRW}}(t,R)$ is peaked at

$$\tau_{\text{typ}}(R) \simeq \tau_0 (R/a)^{2/\mu}. \quad (10)$$

The corresponding cumulative FPT distribution takes the form

$$C_{\text{CTRW}}(t,R) = \int_t^\infty dt' F(t',R) = \hat{C}(tR^{-2\mu}). \quad (11)$$

Here $\hat{C}(z) = \int_z^\infty dy\, \mu y^{-\mu-1} \Phi(y)$. For $z \gg 1$, $\hat{C}(z) \simeq \Phi_\infty z^{-\mu}$.

B. The FPT distribution in the QTM

Equation (5) integrated over t is a special example of a general formula for the cumulative FPT distribution

$$C(t,R) = \sum_\Gamma W_\Gamma C_\Gamma(t), \quad (12)$$

where the summation extends over all possible lattice walks Γ connecting the launch site to the target. Here W_Γ is the probability for a path Γ in the lattice walk, with the normalization $\sum_\Gamma W_\Gamma = 1$, and $C_\Gamma(t)$ the probability that the total passage time exceeds t. In terms of the sojourn time distribution $P_i(t)$ on site i, we may write

$$C_\Gamma(t) = \int H\left(t - \sum_{i\in\Gamma} t_i\right) \prod_{i\in\Gamma} P_i(t_i) dt_i, \quad (13)$$

where $H(t)$ is the Heaviside step function.

For the CTRW, the sojourn time distributions $P_i(t)$ are identical for all sites. Hence $C_\Gamma(t)$ depends only on the path length N, in which case paths with the same N can be grouped together, leading to Eq. (5). On the other hand, $C_\Gamma(t)$ for the QTM depends on the actual sites visited. An interesting question is whether the disorder-averaged $C_\Gamma(t)$ depends only on the path length N_Γ but not its spatial trajectory. If so, the ensemble-averaged $C(t,R)$ can again be cast in the form of Eq. (5).

The answer to the above question is in the affirmative if, on the lattice walk Γ, each site visited appears only once, i.e., there is no return to any given site on the path. For this group of lattice walks, the disorder-averaged $C_\Gamma(t)$ is equivalent to its annealed counterpart whose sojourn time distribution is given by

$$\langle P_i(t) \rangle = \int_1^\infty \frac{e^{-t/\tau}}{\tau} \frac{\mu d\tau}{\tau^{\mu+1}} = \mu t^{-\mu-1} \int_0^t x^\mu e^{-x} dx. \quad (14)$$

Here and elsewhere we use $\langle \cdot \rangle$ to denote the average over the quenched disorder. It is easy to verify that Eq. (14) also has a fat tail that decays as $t^{-\mu-1}$ at large t.

The theory of lattice random walks [28,29] can be applied to calculate the distribution of returns for the setup illustrated in Fig. 1. For $d < 2$, the typical number of returns grows with R as R^{2-d} (logarithmic at $d = 2$). Hence a different scheme to compute the ensemble average of $C(t,R)$ is required. On the other hand, for $d > 2$, the return distribution decays exponentially. Furthermore, the majority of returns to a given site take place in a short section of the walk, allowing for a renormalization group treatment of their effects on $C_\Gamma(t)$ [19]. In the following, however, we will take a different route to reorganize terms in Eq. (12) to compute $C(t,R)$, focusing on contributions from the deepest traps.

The calculation in Appendix A shows that $C_\Gamma(t)$ has an exponential tail with a time constant $\tau_\Gamma = \sum_{i\in\Gamma} \tau_i$. Furthermore, under Eq. (2) at $\mu < 1$, τ_Γ is dominated by the largest trapping constant $\tau_{\max,\Gamma} = \max_{i\in\Gamma}\{\tau_i\}$. These observations suggest that $C_\Gamma(t)$ may be replaced by the cumulative sojourn time distribution at the deepest trap on path Γ. More precisely, labeling each path Γ by $\tau_{\max,\Gamma}$, we rewrite Eq. (12) as

$$C(t,R) = \sum_i C_i(t,R), \quad (15)$$

where the partial sum

$$C_i(t,R) = \sum_{\Gamma, i\in\Gamma, \tau_i = \tau_{\max,\Gamma}} W_\Gamma C_\Gamma(t) \quad (16)$$

is restricted to paths Γ that go through site i with τ_i the largest trapping constant on Γ.

To proceed further, we introduce a single-trap model where $\tau_j = \tau_0$ for all sites except at site i located a distance r from the center of the sphere, for which $\tau_i = \tau_Q \gg \tau_0 (R/a)^2$. In Appendix B we present a calculation of the probability that the trap is visited by a first-passage trajectory illustrated in Fig. 1,

$$w(r,R) \simeq (1 - f_d) \frac{2d}{S_d} \frac{r^{2-d} - R^{2-d}}{d-2} \quad (1 \ll r < R). \quad (17)$$

Here f_d is the probability of return on an infinite lattice and $S_d = 2\pi^{d/2}/\Gamma(d/2)$ is the surface area of unit sphere. For simple cubic lattice, $f_3 \simeq 0.34$. Taking into account multiple visits [28], the calculation yields an exponential tail for the cumulative FPT distribution with a renormalized time constant

$$C_1(t,R|\tau_Q,r) \simeq w(r,R) \exp(-e_d t/\tau_Q), \quad (18)$$

where $e_d \equiv 1 - f_d$ is the probability of no return. Contributions from paths that do not go through the trap die out at times much shorter than τ_Q.

We now compare Eq. (16) with (18) when the site i corresponds to the deepest trap in the system, with $\tau_i = \tau_Q$. In this case, the sum in Eq. (16) includes all paths that go

through site i, as in the single-trap model. The total time spent on other sites on the path is of the order of $\tau_{\rm typ}(R)$ in Eq. (16) and $\tau_0(R/a)^2$ in the single-trap model, respectively. Hence, in both cases, the total passage time is well approximated by the sojourn time on the deepest trap. This allows us to write, for the deepest trap,

$$C_i(t,R) \simeq C_1(t,R|\tau_i,r_i), \tag{19}$$

where r_i is the distance of site i to the origin.

For the second deepest trap in the system, the same argument leading to (19) applies except that the right-hand side of the equation contains extra contributions from paths that visit both the deepest and the second deepest trap. To eliminate such terms, we need to replace $w(r,R)$ in Eq. (18) with $w(i,j,R)$, which gives the probability of reaching the boundary via site i with an absorbing site at j. Continuing the procedure to the $(n+1)$th deepest trap, one needs to compute the visit probability to the site in question in the presence of n absorbing sites and the system boundary, which is quite challenging. However, using the annealed approximation that, in each step, the walker has a probability $p = n/\mathcal{N}$ to run into one of these sites, we obtain the survival probability $(1-p)^N \simeq \exp(-nN/\mathcal{N})$ in an N-step walk. Applying this estimate to first-passage trajectories with $N \simeq R^2$, we see that Eq. (19) holds approximately when $n < n_c = \mathcal{N}/N \simeq (R/a)^{d-2}$, but for weaker traps, $C_i(t,R)$ diminishes rapidly. The trapping time constant at n_c satisfies $(\tau/\tau_0)^{-\mu} = n_c/\mathcal{N} = (R/a)^2$, yielding a cutoff time constant $\tau_{\rm typ}(R)$ given by Eq. (10).

The above discussion yields the following approximate expression for the probability that the FPT in a given sample is greater that t,

$$C_{\rm QTM}(t,R) \simeq \sum_{i,\tau_i>\tau_{\rm typ}(R)} C_1(t,R|\tau_i,r_i), \tag{20}$$

where $C_1(t,R|\tau_i,r_i)$ at $t > \tau_{\rm typ}(R)$ is given by Eq. (18). Each term in the sum decays exponentially with a time constant given by the strength of the trap. The largest time constant is set by the deepest trap in the system.

Given the simple mathematical form of Eq. (20), various properties of the QTM can be derived analytically. For example, as we show in Appendix C, the mean and variance of $C(t,R)$ over different disorder realizations are easily computed. For $2 < d < 4$, the results are given by

$$\langle C(t,R)\rangle \simeq \mu e_d^{1-\mu} R^2 t^{-\mu} \gamma\left(\mu, \frac{e_d t}{R^{2/\mu}}\right), \tag{21}$$

$$\langle [\Delta C(t,R)]^2\rangle \simeq \mu (2e_d)^{2-\mu} S_d^{-1} \frac{d}{4-d} R^{4-d} t^{-\mu} \gamma\left(\mu, \frac{2e_d t}{R^{2/\mu}}\right). \tag{22}$$

Here $\gamma(\mu,z) = \int_0^z dx\, x^{\mu-1}e^{-x}$ is the incomplete gamma function. As expected, the ensemble-averaged FPT distribution (21) is essentially the same as that of the CTRW. On the other hand, its relative fluctuation satisfies the scaling

$$\frac{\langle [\Delta C(t,R)]^2\rangle^{1/2}}{\langle C(t,R)\rangle} = R^{-(d-2)/2} f(tR^{-2/\mu}), \tag{23}$$

where $f(z) \sim z^{\mu/2}$ for $z \gg 1$. The normalized fluctuation is proportional to $(t/\tau_Q)^{\mu/2}$ in the intermediate time regime $\tau_{\rm typ} < t < \tau_Q$ and becomes of order 1 or bigger when t exceeds τ_Q.

IV. SIMULATION RESULTS

We performed extensive kinetic Monte Carlo simulations of the CTRW and the QTM on the three-dimensional simple cubic lattice to verify the analytic results presented in Sec. III. In each run, a particle is released from the origin at $t = 0$ and performs an unbiased random walk through nearest-neighbor hops. The walk is terminated when the particle, for the first time, reaches a site at a distance greater than R from the origin. The total passage time is given by the sum of sojourn times at each stop along the path. In the case of the CTRW, the sojourn times are drawn independently from the distribution (2). For the QTM, a set of trapping time constants τ_i is first assigned to the lattice sites. The actual sojourn time upon each visit to a given site follows an exponential distribution with the preassigned time constant. The system sizes investigated are from $R = 7$ to 15.

A. The FPT distribution

Figure 2 shows three examples for the cumulative distribution function $C(t,R)$ at $R = 7$ and $\mu = 0.71$. Here $\tau_{\rm typ} = R^{2/\mu} = 240$ in units chosen. More than 10^6 trajectories are generated to obtain accurate statistics. As can be seen from the figure, for both the CTRW and the QTM, $C(t,R)$ begins to drop from its maximum value 1 around $\tau_{\rm typ}$. The shape of $C(t,R)$ from the two samples in the QTM is quite similar for t around $\tau_{\rm typ}$, confirming that the most probable value of the FPT in the QTM does not vary significantly from sample to sample and coincides with its annealed counterpart CTRW. In the tail part of the FPT distributions, however, the two samples in the QTM show progressively larger deviations from the power law $C(t,R) \simeq R^2 t^{-\mu}$ (dash-dotted line) that describes well the CTRW data. At very long times, $C(t,R)$ from the QTM exhibits the exponential decay predicted by the theory

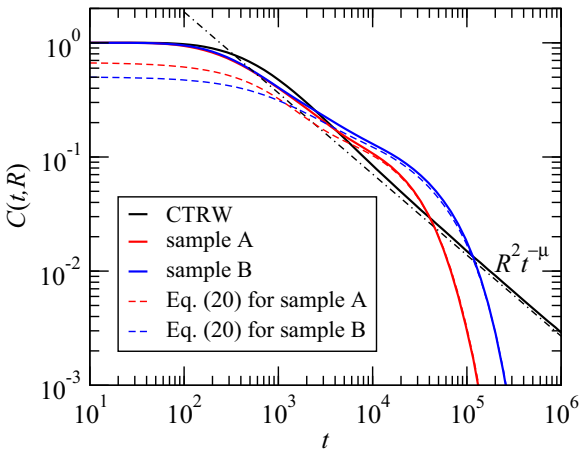

FIG. 2. (Color online) Cumulative distributions of the first-passage time from simulations of the CTRW model and the QTM on the three-dimensional simple cubic lattice. Here $R = 7$ and $\mu = 0.71$. Dashed lines are computed using Eq. (20) for the specific trap configuration in each of the two samples, respectively.

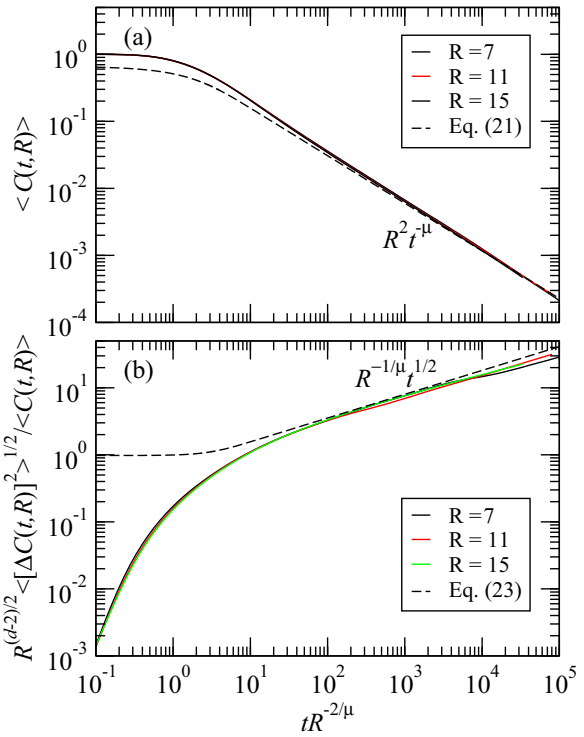

FIG. 3. (Color online) Simulation data of the QTM on the three-dimensional simple cubic lattice at $\mu = 0.71$. (a) Scaling plot of the mean cumulative FPT distribution for three different system sizes $R = 7$ (black line), 11 (red line), and 15 (green line), together with numerical evaluation of Eq. (21) (dashed line). (b) Scaling plot of the relative fluctuation of the cumulative FPT distribution from simulations of the QTM at three different sizes, along with numerical evaluation of Eq. (23).

presented in Sec. III. The tail part of the FPT distribution in each case is well described by Eq. (20).

Figure 3 shows our simulation data for the disorder-averaged $C(t,R)$ and its relative fluctuation from 10 000 realizations of the QTM at the three system sizes $R = 7$, 11, and 15. Also shown are numerical evaluations of the corresponding analytic expressions presented in Sec. III. Excellent data collapse upon scaling of the variables is seen over six decades in time. Both Eqs. (21) and (23) are in quantitative agreement with simulation data on the tail side of the FPT distribution. For $t < \tau_{\rm typ} \simeq R^{2/\mu}$, Eq. (21) yields a value $e_d \simeq 0.66$ less than 1, presumably due to contributions from trajectories not included in the sum (20). The latter is also responsible for the discrepancy between Eq. (23) and the simulation data in the short time regime, where the actual sample-to-sample variations of $C(t,R)$ decrease rapidly due to self-averaging. Taken together, the simulation results confirm quantitatively the decomposition scheme (20) for the tail of the FPT distribution in the QTM.

B. Hit map

We have also monitored the statistics of the end position of the first-passage trajectories as a function of the passage time t. This defines a time-dependent hit map on the absorbing surface. For the CTRW, since the trajectories are spatially independent of each other, the hit map is uniform at all times

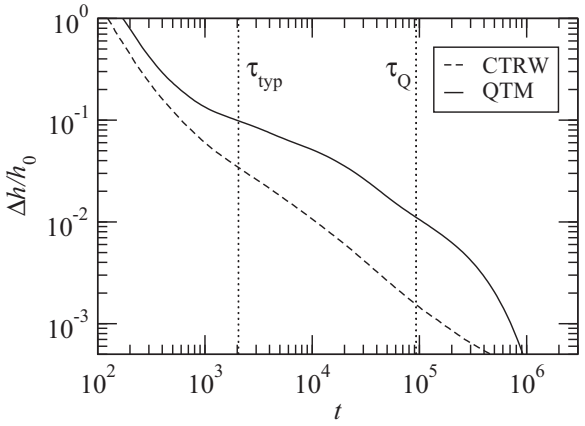

FIG. 4. Relative hit density fluctuation in the CTRW and QTM. Here $R = 15$ and $\mu = 0.71$.

apart from statistical fluctuations when only a finite number of hits are registered. However, the QTM is expected to show a correlated hit density pattern that evolves over time. Sites with long sojourn time constants cause delay to trajectories going through them, thereby casting their shadows on the absorbing surface at short times. At very long times, however, all lattice random walks will have sufficient time to complete their journey and uniformity is restored.

To construct the spatially resolved landing probability on the absorbing surface, we first record $H(\mathbf{x}|t,R)$, the number of hits registered at site $\mathbf{x}$ up to time t. Since a regular lattice is used in the simulations, different surface sites have a different cross section to capture the incoming walkers. To minimize this effect, we performed local averaging by collecting hits into a neighborhood instead of a single site on the boundary. The neighborhood $\Gamma_{\mathbf{x}}$ of a given boundary site $\mathbf{x}$ includes the site itself plus its nearest neighbors and next-nearest neighbors that are also boundary sites. Let $N_{\mathbf{x}}$ be the number of boundary sites in $\Gamma_{\mathbf{x}}$. A coarse-grained hit number is defined as

$$H_{\rm CG}(\mathbf{x}|t,R) = \frac{1}{N_{\mathbf{x}}} \sum_{\mathbf{x}' \in \Gamma_{\mathbf{x}}} H(\mathbf{x}'|t,R). \tag{24}$$

Using the coarse-grained data, we further normalize against $H_{\rm CG}(\mathbf{x}|t=\infty,R)$ to remove the lattice effect, i.e., by introducing the normalized cumulative hits

$$h(\mathbf{x}|t,R) \equiv \frac{H_{\rm CG}(\mathbf{x}|t,R)}{H_{\rm CG}(\mathbf{x}|\infty,R)}. \tag{25}$$

Figure 4 shows the relative spatial fluctuation of $h(\mathbf{x}|t,R)$ in a system of size $R = 15$ by taking statistics over 10^7 launches. Here

$$h_0(t,R) = \langle h(\mathbf{x}|t,R)\rangle_{\mathbf{x}}, \tag{26}$$

$$\Delta h(t,R) = \left[\langle h^2(\mathbf{x}|t,R)\rangle_{\mathbf{x}} - h_0^2(t,R)\right]^{1/2}, \tag{27}$$

where $\langle\cdot\rangle_{\mathbf{x}}$ denotes average over all boundary sites. For both the QTM and the CTRW, the relative fluctuation decreases as the number of hits accumulate. It is also evident that the spatial inhomogeneity is much stronger in the QTM than in the CTRW. Ideally, one expects the hit pattern to saturate around τ_Q when most of the walkers have completed their journey to

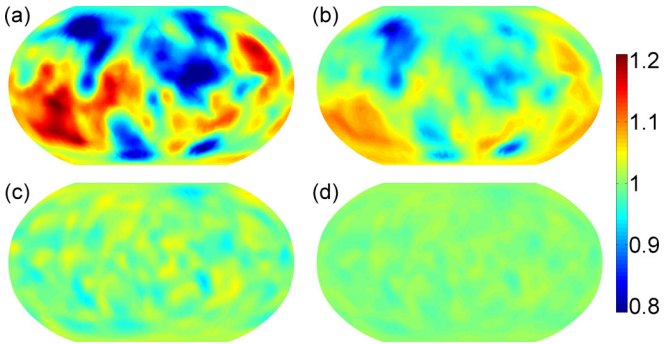

FIG. 5. (Color online) Earth plot of the normalized hit map on the absorbing surface at $R = 15$. Here $\mu = 0.71$. (a) One sample of the QTM at $t = 6200$. (b) Same sample at $t = 20\,000$. (c) CTRW at $t = 6200$. (d) CTRW at $t = 20\,000$.

the absorbing surface. Equation (25) somewhat underestimates this terminal fluctuation by adopting $H_{\rm CG}(\mathbf{x}|\infty, R)$ as the normalization. The latter contains both the lattice effect and residual fluctuations in a finite number of launches.

Figure 5(a) shows the actual hit map

$$h^{\rm r}(\mathbf{x}|t,R) \equiv \frac{h(\mathbf{x}|t,R)}{h_0(t,R)} \tag{28}$$

for the QTM sample at $t = 6200 \simeq 3\tau_{\rm typ}$, where 50% of the launched particles have landed. At this time, maximum density variation on the surface reaches close to 50%. Figure 5(b) shows the hit map of the same QTM sample at a much later time $t = 20\,000 \simeq 10\tau_{\rm typ}$, where about 80% of the particles have arrived. Although the amplitude of the density variation has decreased from Fig. 5(a), the patterns of high and low densities resemble each other. Figures 5(c) and 5(d) show the corresponding maps under the CTRW dynamics, where the density fluctuations are much weaker.

V. CONCLUSION

In this paper we have shown that the QTM above its critical dimension $d_c = 2$ still differs from its annealed counterpart CTRW in the first-passage-time statistics. For power-law distributed sojourn times at $\mu < 1$ where the particle motion becomes subdiffusive, the tail of the FPT distribution for a given sample is well approximated by a sum of exponentials whose time constants are associated with the deepest traps in the system. Intuitively, this behavior can be understood from rare-event statistics where the passage time of each trajectory is dominated by the strongest trap visited by the walker. By grouping trajectories that go through the same trap, one obtains constitutive terms in the FPT distribution, with weights and a renormalized time constant that can be calculated by applying the theory of lattice random walk. The largest time constant in a given sample of linear size R scales with R as $\tau_Q \simeq R^{d/\mu}$. The cutoff time constant $\tau_{\rm typ} \simeq R^{2/\mu}$ for traps that contribute to the summation is the typical FPT in such a system.

A detailed comparison of our analytic expressions against simulations of the QTM shows quantitative agreement in the tail of the FPT distribution. For the peak part of the FPT distribution, however, our treatment is not sufficient to produce quantitatively accurate results, though the predicted scaling with the system size R is well obeyed by simulation data. In the future one may consider improvements of the single-trap approximation by, e.g., replacing contributions from less strong traps by an annealed average with a suitable cutoff, as in the solution of the random energy model [31].

The QTM differs from the CTRW also in the spatially resolved arrival probability on the absorbing boundary, whose relative variation can be as big as 50%. It would be interesting to see if such "shadows" of strong traps can be measured in experiments on, say, the exit statistics of mRNAs through nuclear pores. With sufficient statistics, the exit pattern may enable detection of large-scale movement of chromosomes inside the cell nucleus.

ACKNOWLEDGMENTS

The work was supported in part by the NSFC under Grant No. U1430237 and by the Research Grants Council of the Hong Kong Special Administrative Region (HKSAR) under Grant No. 201910.

APPENDIX A: RARE-EVENT-DOMINATED PASSAGE TIME

To justify the replacement of the total elapsed time of a given passage by the largest sojourn time on the path in our treatment of the CTRW, let us compare the distribution of the sum $t_{\rm sum} = \sum_{i=1}^{N} t_i$ and that of the largest term in the sum $t_{\rm max} = \max_i\{t_i\}$. Denoting by $P(t)$ and $f_N(t)$ the distributions of t_i and $t_{\rm sum}$, respectively, we have

$$f_N(t) = \left\langle \delta\left(t - \sum_{i=1}^{N} t_i\right)\right\rangle, \tag{A1}$$

where angular brackets denote averaging over the distribution of the t_i's. Their Laplace transforms are given respectively by

$$\hat{P}(s) = \int_0^\infty P(t)e^{-st}dt = \langle e^{-st}\rangle, \tag{A2}$$

$$\hat{f}_N(s) = \int_0^\infty \left\langle \delta\left(t - \sum_{i=1}^{N} t_i\right)\right\rangle e^{-st}dt = [\hat{P}(s)]^N. \tag{A3}$$

Consider now the power-law distribution (2) at $\omega_0 = 1$. For $\mu < 1$, its Laplace transform is given by

$$\hat{P}(s) = 1 - \Gamma(1-\mu)s^\mu + \mu\sum_{n=1}^{\infty}\frac{(-1)^{n-1}}{n!}\frac{s^n}{n-\mu}. \tag{A4}$$

For $Ns^\mu \ll 1$ we have $\hat{P}(s) \simeq 1 - \Gamma(1-\mu)s^\mu$ and $\hat{f}_N(s) \simeq 1 - \Gamma(1-\mu)Ns^\mu$. Hence we expect $f_N(t) \simeq N\mu t^{-\mu-1}$ for $t \gg N^{1/\mu}$, in agreement with Eq. (8).

In the QTM, the sojourn times t_i on the path each satisfies its own distribution

$$P_i(t_i) = \tau_i^{-1}\exp(-t/\tau_i) \tag{A5}$$

with a site-dependent time constant τ_i. The Laplace transform (A3) is modified to

$$\hat{f}_\Gamma(s) = \prod_{i\in\Gamma}\frac{1}{1+\tau_i s}. \tag{A6}$$

For small s, we have $\hat{f}_\Gamma(s) \simeq 1 - \tau_\Gamma s$, where $\tau_\Gamma = \sum_{i\in\Gamma} \tau_i$. Hence $f_\Gamma(t)$ decays exponentially at large t with a time constant τ_Γ. In the case when τ_i's are distributed according to Eq. (2), τ_Γ can be approximated by the largest time constant $\tau_{\max,\Gamma}$ on the path. Multiple visits to the deepest trap can also be treated as in Appendix B.

APPENDIX B: SINGLE-TRAP MODEL

In Sec. III B we introduced a single-trap model where the hopping rate $k_i = \tau_0^{-1}$ except at the trap site located at a distance r from the center of a sphere of radius R, where $k_i = \tau_Q^{-1}$. We assume $\tau_Q \gg \tau_0(R/a)^2$ so that the tail of the FPT distribution is dominated by trajectories that make at least one visit to the trap. Here a is the typical distance traveled by the walker in a time τ_0 when outside the trap.

Let us first revisit the problem of a discrete-time random walk on a d-dimensional hypercubic lattice, paying special attention to the presence of an absorbing boundary S. In each step, the walker leave its current site and moves to one of its neighbors with equal probability. The probability $P(\mathbf{x},n)$ that the walker is at site $\mathbf{x}$ after n steps satisfies the lattice diffusion equation

$$P(\mathbf{x},n+1) = \frac{1}{2d} \sum_{\mathbf{x}'\in\text{n.n. of }\mathbf{x}} P(\mathbf{x}',n). \tag{B1}$$

We introduce

$$\Phi(\mathbf{x}) \equiv \sum_{n=0}^{\infty} P(\mathbf{x},n). \tag{B2}$$

For a walker launched from the origin, summing both sides of Eq. (B1) over n yields

$$\frac{1}{2d} \sum_{\mathbf{x}'\in\text{n.n. of }\mathbf{x}} \Phi(\mathbf{x}') - \Phi(\mathbf{x}) = -\delta_{\mathbf{x},0}. \tag{B3}$$

Here $\delta_{\mathbf{x},0} = 1$ if $\mathbf{x}$ is at the launch site and zero otherwise. Equation (B3) is a lattice version of the Poisson equation whose continuum limit takes the form

$$\frac{1}{2d}\nabla^2\Phi = -\delta(\mathbf{x}). \tag{B4}$$

The solution of Eq. (B4) with the boundary condition $\Phi(|\mathbf{x}| = R) = 0$ is given by

$$\Phi(\mathbf{x}) = \frac{2d}{S_d}\frac{1}{d-2}\left(\frac{1}{|\mathbf{x}|^{d-2}} - \frac{1}{R^{d-2}}\right). \tag{B5}$$

Here $S_d = 2\pi^{d/2}/\Gamma(d/2)$ is the surface area of a unit sphere in d dimensions.

We now compute the probability $Q(\mathbf{x},n)$ that the walker, launched from the origin, arrives at site $\mathbf{x}$ for the first time in n steps. Quite generally, we may write

$$P(\mathbf{x},n) = \sum_{n'=1}^{n} Q(\mathbf{x},n')U(\mathbf{x},n-n') \quad (n>0). \tag{B6}$$

Here $U(\mathbf{x},n)$ is the probability that a walker launched from $\mathbf{x}$ returns to the same site in n steps. Summing both sides of Eq. (B6) over n, we obtain

$$\Phi(\mathbf{x}) = \delta_{\mathbf{x},0} + \Psi(\mathbf{x}) \sum_{n=0}^{\infty} U(\mathbf{x},n), \tag{B7}$$

where

$$\Psi(\mathbf{x}) \equiv \sum_{n=1}^{\infty} Q(\mathbf{x},n) \tag{B8}$$

is the probability that the walker visits site $\mathbf{x}$ before being absorbed by the boundary S. Applying Eq. (B7) to the site $\mathbf{x} = 0$, we obtain the probability of return

$$\Psi(0) = 1 - \frac{1}{\Phi(0)}. \tag{B9}$$

For $d > 2$, $P_0 \equiv \lim_{R\to\infty}\Phi(0)$ is finite. Hence Pólya's random-walk constant $f_d \equiv \Psi(0) = 1 - 1/P_0$ is less than one. Equivalently, the probability of no return $e_d = 1 - f_d > 0$. In general, the probability of precisely k returns is given by

$$f_{d,k} = (f_d)^k e_d. \tag{B10}$$

When the absorbing boundary S is at a finite distance, the above results acquire a correction that essentially goes down as ξ^{2-d}, where ξ is the distance to the nearest point on the boundary. Ignoring such corrections, we may approximate $U(\mathbf{x},n)$ by $P(0,n)$. Consequently, Eq. (B7) yields

$$\Psi(\mathbf{x}) \simeq \frac{\Phi(\mathbf{x})}{\Phi(0)} \equiv w(|\mathbf{x}|,R) \quad (\mathbf{x}\neq 0). \tag{B11}$$

Here

$$w(r,R) = (1-f_d)\frac{2d}{S_d}\frac{1}{d-2}\left(\frac{1}{r^{d-2}} - \frac{1}{R^{d-2}}\right) \tag{B12}$$

is the probability to visit a site at distance r from the launch site, in the presence of the absorbing sphere of radius R. Returning to the lattice walk, the divergence of Eq. (B12) at small distances should be truncated when r becomes comparable to the lattice constant.

We now return to the single-trap model where the sojourn time t spent by the walker upon each visit to the trap satisfies the distribution

$$p(t) = \tau_Q^{-1}\exp(-t/\tau_Q). \tag{B13}$$

Under the assumption that τ_Q is much greater than the typical FPT to the boundary when trap is not visited, we may write the FPT distribution of the single-trap model as

$$F_1(t) \simeq [1 - w(r,R)]\delta(t) + \sum_{k=1}^{\infty} w_k(r,R)\left\langle \delta\left(t - \sum_{j=1}^{k} t_j\right)\right\rangle. \tag{B14}$$

Here the angular brackets indicate an average over the sojourn times $\{t_j\}$ distributed according to (B13) and

$$w_k(r,R) = (f_d)^{k-1}e_d w(r,R) \quad (k>0) \tag{B15}$$

is the probability that the trap is visited exactly k times before the walker reaches the boundary S.

The Laplace transform of Eq. (B14) is given by

$$\hat{F}_1(s) = 1 - w(r,R) + \sum_{k=1}^{\infty} w_k(r,R) \prod_{j=1}^{k} \langle e^{-st_j} \rangle. \quad \text{(B16)}$$

From Eq. (B13) we obtain $\langle e^{-st} \rangle = 1/(1 + s\tau_Q)$. With the help of Eq. (B15) we then have

$$\hat{F}_1(s) = 1 - w(r,R) + e_d w(r,R) \frac{1}{e_d + s\tau_Q}. \quad \text{(B17)}$$

Consequently,

$$F_1(t) \simeq [1 - w(r,R)]\delta(t) + w(r,R) \frac{e_d}{\tau_Q} \exp(-e_d t/\tau_Q). \quad \text{(B18)}$$

See also Ref. [24] for a general discussion on the decomposition. Integrating the tail of the distribution, we obtain Eq. (18).

APPENDIX C: STATISTICS OF $C(t,R)$ IN THE QTM

The sum in Eq. (20) is restricted to sites with $\tau_i > \tau_{\rm typ}(R)$. Alternatively, we may extend the sum to all sites inside the sphere, where a given site i contributes a term

$$c_i(t) = \begin{cases} w(r_i,R) e^{-e_d t/\tau_i} & \text{for } \tau_i > \tau_{\rm typ}(R) \\ 0 & \text{otherwise.} \end{cases} \quad \text{(C1)}$$

The mean and variance of c_i are given by

$$\begin{aligned} \langle c_i(t) \rangle &= \int_{\tau_{\rm typ}(R)}^{\infty} d\tau \frac{\mu}{\tau^{\mu+1}} w(r_i,R) e^{-e_d t/\tau} \\ &= t^{-\mu} w(r_i,R) \frac{\mu}{e_d^{\mu}} \gamma\left(\mu, \frac{e_d t}{\tau_{\rm typ}(R)}\right), \end{aligned} \quad \text{(C2)}$$

$$\begin{aligned} \langle [\Delta c_i(t)]^2 \rangle &= w^2(r_i,R) \left[\int_{\tau_{\rm typ}(R)}^{\infty} d\tau \frac{\mu}{\tau^{\mu+1}} e^{-2e_d t/\tau} \right. \\ &\quad \left. - \left(\int_{\tau_{\rm typ}(R)}^{\infty} d\tau \frac{\mu}{\tau^{\mu+1}} e^{-e_d t/\tau} \right)^2 \right] \\ &= t^{-\mu} w^2(r_i,R) \left[\frac{\mu}{(2e_d)^{\mu}} \gamma\left(\mu, \frac{2e_d t}{\tau_{\rm typ}(R)}\right) \right. \\ &\quad \left. - t^{-\mu} \frac{\mu^2}{e_d^{2\mu}} \gamma^2\left(\mu, \frac{e_d t}{\tau_{\rm typ}(R)}\right) \right]. \end{aligned} \quad \text{(C3)}$$

Here $\gamma(\mu,z) = \int_0^z dx\, x^{\mu-1} e^{-x}$ is the incomplete gamma function. Since the τ_i's are independently chosen from the distribution (2), the c_i's are also statistically independent. Hence the mean and variance of $C(t,R) = \sum_i c_i(t)$ are given by

$$\langle C(t,R) \rangle \simeq \int_{|\mathbf{x}|<R} d^d\mathbf{x}\, t^{-\mu} w(|\mathbf{x}|,R) \frac{\mu}{e_d^{\mu}} \gamma\left(\mu, \frac{e_d t}{\tau_{\rm typ}(R)}\right), \quad \text{(C4)}$$

$$\langle [\Delta C(t,R)]^2 \simeq \int_{|\mathbf{x}|<R} d^d\mathbf{x}\, t^{-\mu} w^2(|\mathbf{x}|,R) \frac{\mu}{(2e_d)^{\mu}} \gamma\left(\mu, \frac{2e_d t}{\tau_{\rm typ}(R)}\right), \quad \text{(C5)}$$

where we have replaced summation over i by integral over space inside the sphere. For $2 < d < 4$, carrying out the integrals over $\mathbf{x}$ yield Eqs. (21) and (22). For $d > 4$, the integral over $\mathbf{x}$ in Eq. (C5) is dominated by contributions close to the origin and hence the lattice cutoff should be considered.

[1] E. Barkai, Y. Garini, and R. Metzler, Phys. Today **65**(8), 29 (2012).
[2] P. C. Bressloff and J. M. Newby, Rev. Mod. Phys. **85**, 135 (2013).
[3] See, e.g., *New Models of the Cell Nucleus: Crowding, Entropic Forces, Phase Separation, and Fractals*, edited by R. Hancock and K. W. Jeon (Academic, New York, 2013).
[4] F. Höfling and T. Franosch, Rep. Prog. Phys. **76**, 046602 (2013).
[5] I. Golding and E. C. Cox, Phys. Rev. Lett. **96**, 098102 (2006).
[6] J.-H. Jeon, V. Tejedor, S. Burov, E. Barkai, S. Selhuber-Unkel, K. Berg-Sørensen, L. Oddershede, and R. Metzler, Phys. Rev. Lett. **106**, 048103 (2011).
[7] B. B. Mandelbrot and J. W. Van Ness, SIAM Rev. **10**, 422 (1968).
[8] E. Lutz, Phys. Rev. E **64**, 051106 (2001).
[9] A. Weron, Phys. Rev. E **71**, 016113 (2005).
[10] J.-H. Jeon, N. Leijnse, L. B. Oddershede, and R. Metzler, New J. Phys. **15**, 045011 (2013).
[11] M. Weiss, Phys. Rev. E **88**, 010101(R) (2013).
[12] E. W. Montroll and G. H. Weiss, J. Math. Phys. **6**, 167 (1965).
[13] J.-H. Jeon, E. Barkai, and R. Metzler, J. Chem. Phys. **139**, 121916 (2013).
[14] M. J. Saxton, Biophys. J. **66**, 394 (1994).
[15] S. Havlin and D. Ben-Avraham, Adv. Phys. **51**, 187 (2002).
[16] H. Li, S.-X. Dou, Y.-R. Liu, W. Li. P. Xie, W.-C. Wang, and P.-Y. Wang, J. Am. Chem. Soc. **137**, 436 (2015).
[17] R. Metzler, J.-H. Jeon, A. G. Cherstvy, and E. Barkai, Phys. Chem. Chem. Phys. **16**, 24128 (2014); A. G. Cherstvy, A. V. Chechkin, and R. Metzler, Soft Matter **10**, 1591 (2014).
[18] J. P. Bouchaud and A. Georges, Phys. Rep. **195**, 127 (1990).
[19] J. Machta, J. Phys. A **18**, L531 (1985).
[20] C. Monthus, Phys. Rev. E **67**, 046109 (2003).
[21] E. M. Bertin and J. P. Bouchaud, Phys. Rev. E **67**, 026128 (2003).
[22] S. Burov and E. Barkai, Phys. Rev. Lett. **106**, 140602 (2011); Phys. Rev. E **86**, 041137 (2012).
[23] L. Luo and L.-H. Tang, Chin. Phys. B **23**, 070514 (2014).
[24] O. Bénichou, C. Chevalier, J. Klafter, B. Meyer, and R. Voituriez, Nat. Chem. **2**, 472 (2010); B. Meyer, C. Chevalier, R. Voituriez, and O. Bénichou, Phys. Rev. E **83**, 051116 (2011); O. Bénichou and R. Voituriez, Phys. Rep. **539**, 225 (2014).
[25] H. Krüsemann, A. Godec, and R. Metzler, Phys. Rev. E **89**, 040101(R) (2014).
[26] S. Condamin, V. Tejedor, and O. Bénichou, Phys. Rev. E. **76**, 050102(R) (2007).
[27] L.-H. Tang and H. Chaté, Phys. Rev. Lett. **86**, 830 (2001).
[28] E. W. Montroll, J. SIAM **4**, 241 (1956).
[29] S. Redner, *A Guide to First-Passage Processes* (Cambridge University Press, Cambridge, 2007).
[30] S. Condamin, O. Bénichou, and J. Klafter, Phys. Rev. Lett. **98**, 250602 (2007).
[31] B. Derrida, Phys. Rev. B **24**, 2613 (1981); B. Derrida and H. Spohn, J. Stat. Phys. **51**, 817 (1988).